# Influence of Shear on the Alignment of a Lamellae-Forming Pentablock Copolymer

**M. E. Vigild,[†] C. Chu,[‡] M. Sugiyama,[§] K. A. Chaffin,[||] and F. S. Bates***

*Department of Chemical Engineering and Materials Science, University of Minnesota, Minneapolis, Minnesota 55455*

*Received April 21, 2000; Revised Manuscript Received October 16, 2000*

ABSTRACT: We characterize shear-induced states of order and disorder in a symmetric lamellae forming poly(cyclohexylethylene) (C)−polyethylene (E) CECEC pentablock copolymer. When subjected to a large amplitude reciprocating shear strain ($\gamma = \pm 600\%$) in the ordered lamellae state, the sample rapidly aligns in a perpendicular orientation with long-range order. The order−disorder transition temperature $T_{ODT}$-($\dot{\gamma}$) decreases with increasing shear rate $\dot{\gamma}$, such that a shear rate of $\dot{\gamma} = 7 \pm 1\ s^{-1}$ is sufficient to disorder the material nearly 30 °C below the quiescent $T_{ODT}$. Small-angle neutron scattering (SANS) from the sheared disordered state displays a symmetry that suggests a fundamentally different influence of shear compared to earlier observations of shear-induced anisotropy in the disordered states of lamellae forming diblock and triblock copolymers. Abrupt cessation of shear leads to spontaneous lamellar ordering into a macroscopically well-aligned transverse orientation—an arrangement that previously has been inaccessible via processing. In contrast to this behavior, the perpendicular alignment forms when cooling the sample from above the $T_{ODT}$ while applying low shear rates, similar to the response of di- and triblock copolymers. These findings shed fresh insight into the complex phenomena that govern flow- and deformation-induced alignment of block copolymer melts.

## 1. Introduction

It is well-known that shear flows can cause microphase-separated block copolymers to align in single crystallike domains with long-range translational order.[1−3] This makes this class of materials interesting for its potential use in nanostructural engineering where control and manipulation of material properties through anisotropic structural elements are relevant to practical applications. In recent years lamellar diblock copolymer melts subjected to shearing have been studied intensively.[4−11] The behavior of block copolymers in a flow field involves complex phenomena that depends on at least three externally controlled parameters, namely, temperature $T$, shear strain $\gamma$, and deformation rate (i.e., frequency $\omega$ for dynamical oscillatory shear flow or shear rate $\dot{\gamma}$ for reciprocating steady shear flow). The proximity of the processing temperature to the order−disorder transition (ODT) of the sample and the deformation rate are the primary factors that determine the overall microdomain alignment.

For many years, the only known orientation induced in lamellae by an oscillatory shear flow was the parallel variety (see Figure 1a).[2,3] The discovery by Koppi et al. of the perpendicular alignment[4] caused a renewed interest in flow-induced manipulation of the structure of lamellar-forming block copolymers. This alignment (see Figure 1b) was generated by flipping the parallel orientation in response to increasing the shear frequency in a poly(ethylene−propylene)−poly(ethylethylene) (PEP−PEE) sample near the $T_{ODT}$. However, Winey and co-workers observed a flip in a polystyrene-polyisoprene (PS−PI) sample from perpendicular to parallel with increasing frequency,[5,12] which apparently contradicts the findings of Koppi et al. Much additional research has generated a conceptual framework that includes at least three orientation regimes in these systems at temperatures close to $T_{ODT}$,[7,8,13,14] which are separated by the characteristic frequencies $\omega_d$ and $\omega_c$, that can be determined by dynamic mechanical spectroscopy.[11,15] (Throughout the literature on this subject, and here, the nonlinear viscoelastic properties at $\dot{\gamma}$ have been related to the linear behavior at $\omega$, based on the empirical Cox−Merz rule.[16]) The shear stable alignment is parallel at low frequencies below $\omega_d$, where the

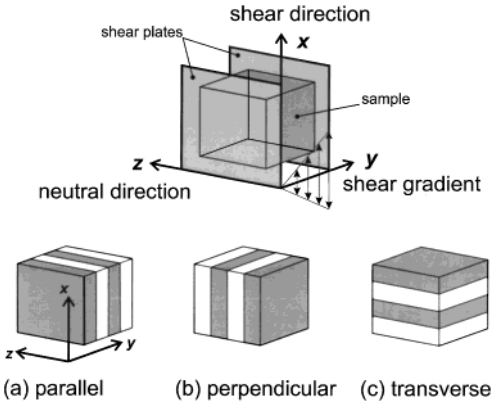


**Figure 1.** Three orthogonal orientations of the lamellar microstructure with respect to the imposed shear. The geometry of the shear plates (shown at the top) identifies the shear direction *x*, the shear gradient direction *y*, and the neutral or vorticity direction *z*. (a) Parallel lamellae with the layer normal aligned parallel to the shear gradient *y*. (b) Perpendicular lamellae with the layer normal aligned parallel to the vorticity direction *z*. (c) Transverse lamellae with the layer normal aligned parallel to the shear direction *x*.

* Corresponding author.
[†] Current address: Department of Chemical Engineering, Technical University of Denmark, 2800 Lyngby, Denmark.
[‡] Current address: Infineum USA L.P., 1900 East Lynden Av., Lynden, NJ 07036.
[§] Current address: Division of Chemistry and Physics of Condensed Matter, Kyushu University, Kyushu, Japan.
[||] Current address: Medtronic Inc., 6700 Shingle Creek Parkway, Brooklyn Center, MN 55430.

10.1021/ma000709q CCC: $20.00 
Published on Web 01/20/2001

viscoelastic properties are governed by the collective relaxation of numerous lamellae organized into a polygrain structure. In the intermediate region between $\omega_d$ and $\omega_c$, the perpendicular alignment is stable. The response in the intermediate region is believed to be controlled by the dynamics of individual lamellae. In the high-frequency spectrum above $\omega_c$, the shear-stable alignment is parallel, and the rheology is influenced by the distortion and relaxation of single molecules.

The third possible orientation of the lamellae is the transverse alignment, where the layer normal is parallel to the direction of shear (see Figure 1c). Transverse lamellae have never been observed as a stable alignment in response to a shearing process, although this orientation has been deduced to be a transient structure in certain time-resolved experiments. Zhang et al.[17] observed a mixed morphology of transverse and parallel components that developed into an alignment dominated by the parallel component when subjected to extended periods of oscillatory flow at a modest strain amplitude ($|\gamma| = 30\%$). Chen et al.[13] used real-time birefringence to study the progress of shear-induced alignment under these conditions. In the high shear frequency regime ($\omega > \omega_c$), a transformation of unaligned regions was seen, which predominantly gave a parallel and transverse alignment. This happened during an initial "fast" process, followed by a late stage "slow" process during which the transverse projection was eliminated. Similar biaxial textures have also been reported by Okamoto et al.[18] and Pinheiro et al.[19] Medium-amplitude oscillatory shear ($|\gamma| \approx 50\%$) induced both the parallel and transverse orientations, which after the cessation of shear and subsequent annealing relaxed toward parallel lamellae by losing the transverse projection of the alignment. (The term "large amplitude" shear widely covers shearing of strains in the nonlinear regime. In this report, we prefer to use it to describe reciprocating or oscillatory flows with at least one rotation around the vorticity axis, i.e., $|\gamma| \geq \pi$. Shears of smaller strains are denoted "medium amplitude", and deformations within the linear viscoelastic regime are referred to as "low amplitude").

The bulk of the research in this field has focused on the effects of alignment by dynamical oscillatory shear fields at temperatures below $T_{ODT}$ and at typical maximum shear strains $|\gamma|$ less than 100%. In some shear studies, much larger strain amplitudes (500−600%) were applied in simple sawtooth reciprocating shear at temperatures both below and above the $T_{ODT}$.[20−23] These strains produce nearly a double rotation around the vorticity direction, and accordingly, these experiments produce flow effects that qualitatively resemble the conditions of simple steady shear. The physics of shearing changes completely when shear is applied in the disordered state, and interesting phenomena are observed when shearing above but close to the $T_{ODT}$, where composition fluctuations dominate the state of the sample. Koppi et al.[20] used a steady reciprocating shear of $|\gamma| = 500\%$ to induce the perpendicular state of a lamellar PEE−PEP diblock copolymer at temperatures a few degrees above $T_{ODT}$. This result confirmed a theoretical prediction by Cates and Milner[24] that steady shear will raise the isotropic-to-lamellar transition temperature by suppression of composition fluctuations. Tepe et al.[23] observed a similar perpendicular alignment when cooling below $T_{ODT}$ at a fixed shear rate in a symmetric PEP−PEE−PEP triblock copolymer. However, with the triblock copolymer, the parallel orientation was the shear stable alignment in the microphase-separated state, contrary to what was found with the analogous diblock copolymer. In contrast to this result Riise et al.[25] reported that another lamellar ABA triblock system (PS−PI−PS) only exhibited the perpendicular behavior. Moreover, in the same report, the authors claimed that the equivalent lamellar PS−PI diblock system yielded the same perpendicular result.

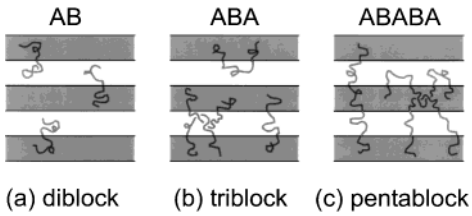


**Figure 2.** Effect of interlayer cross-linking by multiblock copolymers. (a) In melts of diblock copolymers, no domains are connected by bridging blocks. (b) The middle block of triblocks can reside in either the looped or the bridged conformation, which will result in trans-domain coupling of end-block lamellae and high level of mechanical contrast. (c) For pentablock copolymers, all domains are linked together as a result of the molecular architecture, due to either bridging or entangled looping block segments resulting in low mechanical contrast.

Tepe et al. also measured the response of the disordered state of the PEP−PEE−PEP sample to reciprocating shear ($|\gamma| = 600\%$), and found no shear-induced ordering. Instead, shearing disrupted the ordered lamellar structure when applied at temperatures below the quiescent ODT. Different shear-induced behavior below $T_{ODT}$ of di- and triblock copolymers[4,23] and variations and potential conflicts in the reported behavior of triblock copolymers of different designs[23,25] underscore the complex nature of the processes responsible for selecting a particular state of orientation. Obviously, the molecular architecture of triblocks results in bridging and entangled looping by the middle block, which drastically reduces its ability to deform, resulting in "mechanical contrast" between center and end block domains. Other important parameters are the proximity of the glass transition and entanglement effects that also contribute to the block copolymer mechanical, or viscoelastic, contrast.[12,26]

To better address the critical issue of mechanical contrast, we have designed a new CECEC pentablock copolymer comprised of poly(cyclohexylethylene) (C) and polyethylene (E). The pentablock architecture ensures that every domain contains, on average, at least 50% bridging or looping blocks. Both of these should behave like trans-domain cross-linkers. Thus, a lamellar-forming pentablock should offer a unique opportunity to probe the dynamic response in the limit of complete mechanical coupling in the melt state. Figure 2 compares the state of mechanical coupling between layers in diblocks (no coupling), triblocks (partial coupling), and pentablocks (full coupling). We have investigated the alignment of the CECEC sample in the ordered state, studied how the order−disorder transition is affected by steady reciprocating shear ($|\gamma| = 600\%$), and examined the influence of shear on the state of the sample in the disordered phase near the ODT. These results and the associated analysis provide fresh insights into the single chain and cooperative mechanics responsible for microdomain alignment in all these types of block copolymers. Our presentation is organized as follows: Section 2 outlines the experimental techniques

and procedures used in this work. The results are presented in section 3 along with an analysis, followed by a discussion of our findings in the broader context of linear macromolecules in section 4. We summarize our work in section 5.

## 2. Experimental Section

The CECEC pentablock copolymer was synthesized using three basic procedures: (i) sequential anionic polymerization of styrene (S) and butadiene (B) to yield a symmetric living SBS triblock copolymer; (ii) coupling of this product, leading to an SBSSBS pentablock copolymer; (iii) two-step catalytic saturation to the corresponding poly(cyclohexylethylene) (C)−polyethylene (E) pentablock product containing a completely hydrogenated polyethylene block [$C_4H_8$] and a partially deuterated poly(cyclohexylethylene) block [$C_8H_nD_{14-n}$], where $n \approx 5.5$ based on a prior study.[27] The stoichiometric weight fraction of poly(1,4-butadiene) was $w_B = 0.47$. On the basis of a partial deuteration of the C block given by Gehlsen et al.[27] and published mass densities of the hydrogenous block densities at 140 °C ($\rho_E = 0.785$ g/cm$^3$ and $\rho_C = 0.920$ g/cm$^3$ [28]), the volume fraction of polyethylene was $f_E = 0.49$. The stoichiometric number-average molar mass was $M_n = 52\,300$ g/mol with a polydispersity index of $M_w/M_n = 1.04$, given by gel permeation chromatographic (GPC) traces of the unsaturated SBSSBS precursor polymer using polystyrene calibration standards. GPC measurements were made on a Waters 150C instrument operated with a tetrahydrofuran (THF) mobile phase at 30 °C. On the basis of these results the amount of residual SBS triblock was less than 5% by weight.

**Polymerization.** The synthesis procedure was as follows. Rigorously purified styrene monomer (Aldrich Chemical Co.) was initiated with *sec*-butyllithium (Aldrich Chemical Co.) and polymerized in purified cyclohexane at 40 °C under an argon atmosphere. After 4 h, purified 1,3-butadiene monomer (Aldrich Chemical Co.) was added directly to the reactor and polymerization was continued for approximately 12 h at 40 °C. Under these conditions 93% 1,4 and 7% 1,2-addition occurs.[29] Crossover from styryllithium to butadienyllithium was evidenced by a loss of the orange color. The reaction mixture was then cooled to 8 °C, where it was maintained for all subsequent steps. THF was added in a ratio of approximately 50:1 ([THF]:[Li]). Another batch of purified styrene monomer was then added slowly to the reaction mixture with vigorous stirring. The color quickly turned orange, signaling a fast crossover. Under these reaction conditions, the styrene monomer was essentially completely reacted within several minutes of completing monomer addition to the reactor, but to ensure complete conversion, the polymerization was continued for approximately 4 h. Subsequently, a solution of butadiene monomer predissolved in purified THF was added dropwise until the color turned light green. On the basis of the mass of butadiene/THF solution added, the polybutadiene capping sequence was estimated to be four repeat units long. This short capping block facilitates the following coupling reaction. The coupling agent, α,α′-dichloro-*p*-xylene, was introduced dropwise in a purified THF solution. The end point of the coupling reaction was indicated by the disappearance of the light green color characteristic of poly(1,2-butadienyl)-lithium anions in the presence of THF. The resulting SBS′BS pentablock copolymer precursor (here S′ signifies SS) was recovered by precipitation in methanol. (We note that the oligomeric capping block at the center of this polymer is ignored in the remainder of this presentation. Thermodynamic considerations indicate it will not significantly effect the overall morphology or melt dynamics.)

**Two-Step Saturation.** A two-step saturation process was carried out on the SBS′BS pentablock copolymer for the purpose of creating neutron scattering contrast between the blocks of the molecule, by following a method reported by Gehlsen et al.[27,30] First, the B blocks were selectively hydrogenated using a homogeneous Wilkinson's catalyst.[31] The dried SBS′BS pentablock copolymer precursor was dissolved in cyclohexane. The hydrogenation reaction was conducted for 4 h at 100 °C under 100 psi hydrogen pressure. Subsequent NMR analysis (Varian VXR-300) of the recovered SES′ES polymer in perdeuterated benzene [$C_6D_6$] confirmed hydrogenation of more than 99.5% of the carbon−carbon double bonds of the B blocks, while the aromatic unsaturations of the S blocks remained intact. Second, the S blocks were saturated by heterogeneous catalytic deuteration using a novel Pt on $SiO_2$ catalyst.[32] The deuteration reaction was carried out in the cyclohexane solution for 12 h at 177 °C under 500 psi deuterium pressure. All saturation reactions were conducted in a PPI (Precision Pressure Industry) reactor. High-temperature GPC measurements on the totally saturated CECEC block copolymer gave no evidence of chain degradation during the saturation processes.

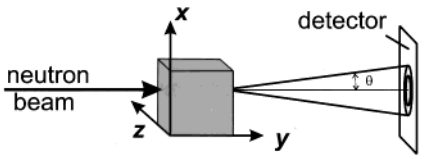


**Figure 3.** Experimental setup of the in situ shearing device. The deformation is defined by the shear direction *x*, the shear gradient *y*, and the neutral direction *z* (see Figure 1). SANS measures scattering in the (*x*,*z*) plane as a function of scattering angle $\theta$. The incident neutron beam is parallel to the shear gradient *y*.

**Mechanical and Structural Characterization.** Solid samples of the neat block copolymer were prepared by compression molding of the precipitated polymer powder. The sample powder was placed in a mold and sandwiched between sheets of Teflon and stainless steel plates. Pressure was applied stepwise (200, 500, and 1000 psi) for 2 min each, at 220 °C. Following cooling to approximately 130 °C a pressure of 1000 psi was held for 2 min before cooling to room temperature. High-temperature GPC measurements on samples taken from the pressed sheets of block copolymer showed no sign of degradation.

Measurements of the dynamic shear storage and loss moduli ($G'$ and $G''$) were made using a Rheometrics RSA II instrument fitted with a shear sandwich fixture. The sample thickness between the shear plates was 0.5 mm. During measurements the sample was kept under a protective temperature controlled nitrogen atmosphere.

Small-angle neutron scattering (SANS) experiments were performed at the National Institute of Standards and Technology (NIST) Center for Neutron Research, Gaithersburg, MD. A neutron wavelength of $\lambda = 6.0$ Å was used with a spread of $\Delta\lambda/\lambda = 0.11$. The sample to detector distance was 4.48 m. Two-dimensional frames of scattering data were recorded and corrected for background scattering and detector response prior to analysis. Each frame was accumulated over 60 s. An in situ reciprocating shear apparatus[4,33] was employed for obtaining SANS patterns while simultaneously deforming the sample. During measurements at high temperatures the apparatus was kept in an environmental chamber filled with helium to prevent sample degradation and reduce loss of neutron beam intensity. A sample thickness of 0.35 mm was maintained by two aluminum plates of dimensions 2.54 cm × 2.54 cm with milled grooves and anodized rails.[34] The deformation of the sample followed a saw tooth profile with a maximum displacement of ±2.1 mm, which gave a maximum strain amplitude of $|\gamma| = 600\%$. Figure 3 shows the experimental setup of the in situ shear device. The shear direction *x* is vertical and the incident neutron beam is parallel with the shear gradient direction *y*.

Small-angle X-ray scattering (SAXS) measurements were performed at the Institute of Technology Characterization Facility at the University of Minnesota. Copper Kα radiation of wavelength $\lambda = 1.54$ Å$^{-1}$ was generated by a Rigaku Ru-200BVH rotating anode using a 0.2 × 2 mm$^2$ microfocus cathode and monochromated by total reflecting Franks mirrors

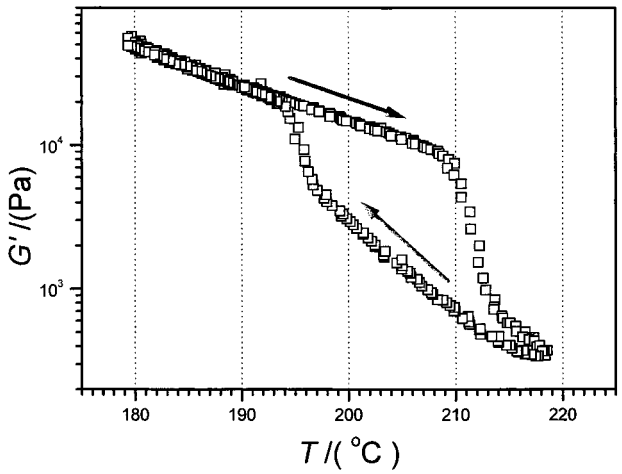


**Figure 4.** Characterization of the order−disorder transition. The arrows indicate data obtained during heating or cooling. The $T_{ODT}$ is evidenced by a drop in elastic modulus $G'$ around 210 °C during heating. The cooling curve shows hysteresis, which indicates some degree of supercooling of the disordered state. Experimental conditions were: heating/cooling rate = 1 °C, oscillating frequency $\omega = 1$ rad/s, and shear strain $|\gamma| = 1\%$.

and a nickel foil filter. Two-dimensional diffraction data were collected with a Siemens HI−STAR multiwire area detector located 231 cm from the sample. All data were corrected for detector response characteristics prior to reduction. The SAXS data were collected at ambient temperature.

Transmission electron microscope (TEM) images were recorded at 120 kV with a JEOL 1210 TEM instrument. Samples were prepared and stained by the technique described by Brown and Butler[35,36] that relies on different degrees of diffusion of the stain into the amorphous poly(cyclohexylethylene) and the semicrystalline polyethylene. A plane surface was cut cryogenically with a glass knife to create a smooth surface for staining in vapors of $RuO_4$. The stained sample was then microtomed (Reichart ultramicrotome) with a diamond knife at ambient temperatures into 80 nm thick sections, that were floated on water and collected on copper TEM grids for analysis by TEM.

## 3. Results and Analysis

**3.1. Linear Dynamic Mechanical Properties.** The thermotropic properties of the pentablock copolymer were characterized by measuring the rheological response while heating and cooling the sample between the ordered and disordered states. The elastic storage modulus $G'$, plotted in Figure 4, shows a significant drop of more than a decade at 210 °C upon heating the sample 1 °C/min at a frequency of $\omega = 1$ rad/s and a shear strain of $|\gamma| = 1\%$. This indicates an order−disorder transition temperature at $T_{ODT} = 210 \pm 2$ °C. Upon cooling at the same rate, the dynamic elastic modulus displays a significant hysteresis, meeting the heating data at $T = 195 \pm 2$ °C. This hysteresis loop shows that the disordered state supercools approximately 15 °C below the equilibrium $T_{ODT}$ under these conditions. A similar behavior has been reported for other block copolymer systems[37] and is attributed to the relatively low rate of nucleation and growth of the ordered state compared to the rate of cooling. Continued cooling of the sample (not illustrated) showed no characteristic features before the temperature equaled the crystallization temperature $T_m = 108$ °C at which point $G'$ significantly increased. There was no indication of a glass transition of the C blocks which could be expected at the bulk value $T_g = 145$ °C.

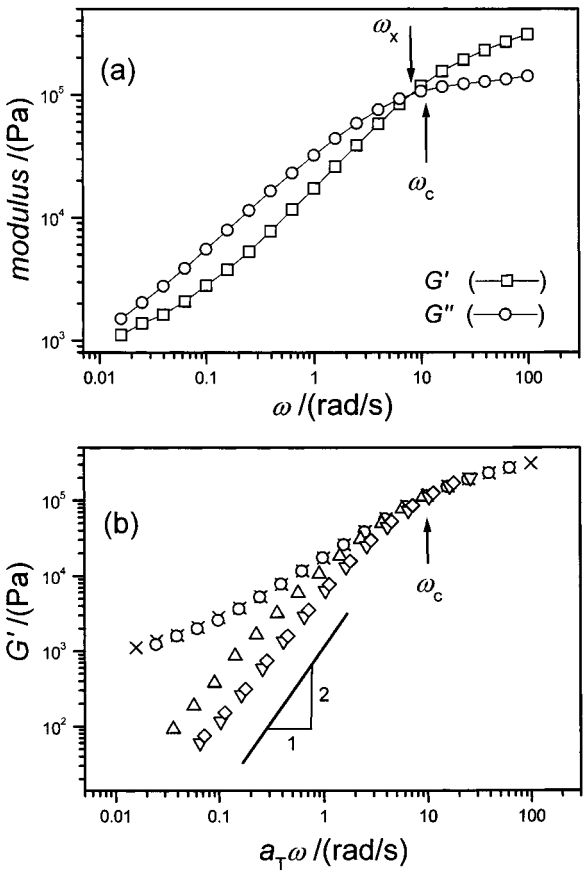


**Figure 5.** Isothermal dynamic viscoelastic properties of CECEC. (a) The frequency dependence of the elastic modulus $G'$ (squares) and the loss modulus $G''$ (circles) of the ordered sample at $T = 199$ °C and $|\gamma| = 1\%$. Arrows indicate the positions of the crossover frequency $\omega_x$ and the characteristic frequency $\omega_c$. (b) TTS plot ($G'$ vs $\omega$) which defines the characteristic frequency $\omega_c$. Frequency sweeps were measured at five temperatures: (×) 199, (○) 204, (△) 209, (▽) 214, and (◇) 219 °C; and shifted by factors $a_T$ to the reference temperature $T = 199$ °C.

The isothermal dynamic viscoelastic properties were probed using frequency sweeps (0.02−100 rad/s) below and above $T_{ODT}$ at a constant strain of $|\gamma| = 1\%$. The response of the sample at 199 °C is shown in Figure 5a. At frequencies $\omega > \omega_x$, $G'$ is greater than the dynamic loss modulus $G''$, while at frequencies $\omega < \omega_x$, $G''$ is greater than $G'$. The crossover frequency $\omega_x$, defined as the point where $G' = G''$, is generally taken as a measure of the longest molecular relaxation time $\tau$. The characteristic frequency $\omega_c$, which we associate with the onset of microdomain dynamics as $\omega$ is reduced,[38] was determined from the time−temperature superpositioning (TTS) of several frequency sweeps at $\omega > \omega_c$. A TTS plot at the reference temperature 199 °C is shown in Figure 5b. Since CECEC is not a rheologically simple material, use of the TTS principle is not rigorously valid.[39] Nevertheless this method of data reduction has been shown to be quite useful in isolating the different dynamic regimes in ordered and disordered block copolymer melts. Within accuracy the characteristic frequency $\omega_c$ is the same as the crossover frequency $\omega_x$. Frequency sweeps of the disordered state showed terminal viscoelastic behavior for a fluid ($G' \sim \omega^2$, and $G'' \sim \omega$ (not shown)) at low frequencies ($\omega \ll \omega_c$).

**3.2. Large Amplitude Steady Reciprocating Shear.** In the following sections, we report the CECEC's

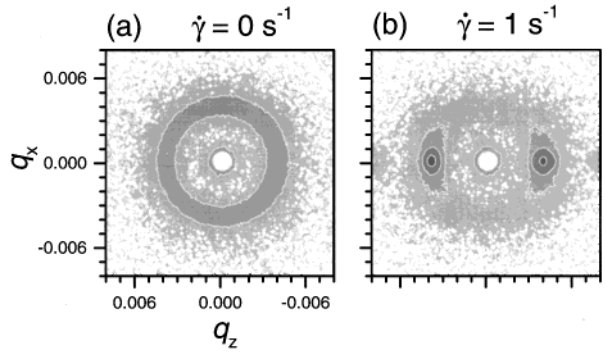


**Figure 6.** Two-dimensional neutron scattering patterns before and after shearing at 183 °C. (a) The isotropically ordered state gives an azimuthally symmetric ring of scattering. (b) The shear-induced ordered state yields well-defined equatorial Bragg reflections of both first and second order, which is associated with a perpendicular lamellae alignment. The SANS intensity is plotted on the same logarithmic scale with one contour level per decade.

sensitivity to shear in both the ordered and disordered states. Our main tools are the in situ shear apparatus and the 2-dimensional SANS instrument that permits the simultaneous imposition of shear while interrogating the associated effects on morphology. Three types of shearing experiments were employed: cooling, heating, and constant temperature. In cooling and heating experiments, the shear rate was fixed and temperature was changed manually in 1 °C stepwise increments with the continuous synchronous collection of data in 60 s intervals. Because of heat transfer limitations the sample temperature lagged slightly behind the set values of the temperature controller, resulting in an error of about 1 °C at any given moment in the experiment. At constant temperature a steady-state response was established based on attainment of an invariant scattering pattern. Transient responses after the abrupt cessation of shear—a fourth type of isothermal experiment referred to as a shear quench—were characterized by recording scattering patterns at regular intervals (60 s) for a period of time.

The SANS experiment measures the scattered intensity $I$ as a function of scattering angle $\theta$ in the $(x,z)$ plane, which coincides with the plane of the shear direction $x$ and the neutral direction $z$ (see Figure 3). The magnitude of the scattering vector $q$ is directly related to the scattering angle by $|q| = 4\pi/\lambda \sin \theta/2$, where $\lambda$ is the radiation wavelength. The two-dimensional SANS data were reduced to one-dimensional form in various ways. Radial plots ($I(q_x)$) or $I(q_z)$) were obtained by azimuthal integration of wedge-shaped sections over in-plane azimuthal angles $\phi$ within ±25° of either the vertical ($x$) or the horizontal ($z$) directions. Circular plots ($I_{q^*}(\phi)$) were obtained by radial integration of the data within a band of ±0.003 Å$^{-1}$ from the scattering peak position $q^*$. Two-dimensional SAXS data were reduced similarly.

**3.2.1. Shear Stable Lamellae at $T < T_{ODT}$.** To determine its response to shear, a compression-molded CECEC sample was loaded into an aluminum shear cell and mounted on the in situ shear apparatus. Any uncontrolled shear alignment due to the loading procedure was erased by disordering the sample at 215 °C. From disorder the sample temperature was set to 183 °C. After thermal equilibration, this resulted in a ring of scattering as shown in Figure 6a. The intensity is approximately twice as great as the ring of scattering produced in the disordered sample, consistent with the development of a microphase-separated structure. The azimuthally symmetric ring shows that there is no orientational preference of the structure. The lack of higher-order reflections indicates that the sample probably contains relatively short-range translational order.

The unaligned state of the ordered morphology was further investigated by TEM of the compression-molded pentablock. A TEM image obtained from a $RuO_4$ stained thin slice of this material is shown in Figure 7a. Consistent with the SANS (and SAXS, not shown) analysis there is no evidence of long-range order, although grains of regular short-range segregation (∼50 nm across) are apparent.

The ordered but unaligned sample was kept at 183 °C in the in situ apparatus, while the shear was activated. The applied shear deformation exposed the sample to a strain amplitude of $|\gamma| = 600\%$ at a shear rate of $\dot{\gamma} = 1.0\ s^{-1}$. Figure 6b illustrates the SANS pattern recorded during the first 60 s of shearing (2.5 complete shear cycles). Microdomain orientation is clearly evidenced by two strong equatorial spots with second-order reflections, consistent with a well-aligned perpendicular lamellar structure (see Figure 1b and additional analysis below). Domain alignment occurred rapidly relative to the time scale of the SANS measurement. Within the first 10 s of the experiment the real-time detector display revealed nearly the full response recorded at 60 s. Continued shearing did not change the scattering data, which indicates that this lamellar orientation is the shear stable morphology of the CECEC sample under these conditions.

**3.2.2. Disorder-to-Lamellae Transition.** Cooling the sample from the disordered state without the application of shear yields a macroscopically isotropic morphology (see Figures 6a and 7a). To see what effect shear has during the isotropic-to-lamellar transition the sample was cooled from disorder while shearing. From an initial temperature $T = 213$ °C the sample was cooled 1 °C/min while collecting SANS data every 60 s. The instrument was set at the relatively low shear rate of $\dot{\gamma} = 0.1\ s^{-1}$. Transformation of the scattering pattern from a circularly symmetric ring into well-resolved equatorial spots and recognizable second-order reflections similar to the data in Figure 6b established the disorder-to-lamellae transition temperature to be $T_{dis-lam} = 195 \pm 1$ °C. This value agrees with the rheological data (see Figure 4). Again, the symmetry of the SANS picture shows that the sample is well ordered and consistent with a perpendicular orientation. This behavior was reproduced while applying greater shear rates ($\dot{\gamma} = 1.0\ s^{-1}$), which provided a protocol for a fast and reliable formation of the well-aligned lamellae by cooling the sample rapidly from disorder to 183 °C while shearing. We used this protocol repeatedly for aligning the sample.

The equatorial spots in the two-dimensional SANS are consistent with the perpendicular orientation, but only project the structure in the $(x,z)$ plane. To support our interpretation of the SANS data, we prepared a separate sample ex situ and examined it by SAXS and TEM. The shear alignment was performed on the RSA II instrument at a frequency of $\omega = 1$ rad/s and strain $\gamma = \pm 99\%$. The sample was loaded and disordered at 220 °C. While shearing, the sample was cooled 2 °C/min to 195 °C where shear was maintained for 1 h. Following the cessation of shear, the sample was cooled to room temperature for structural analysis. Illustrated

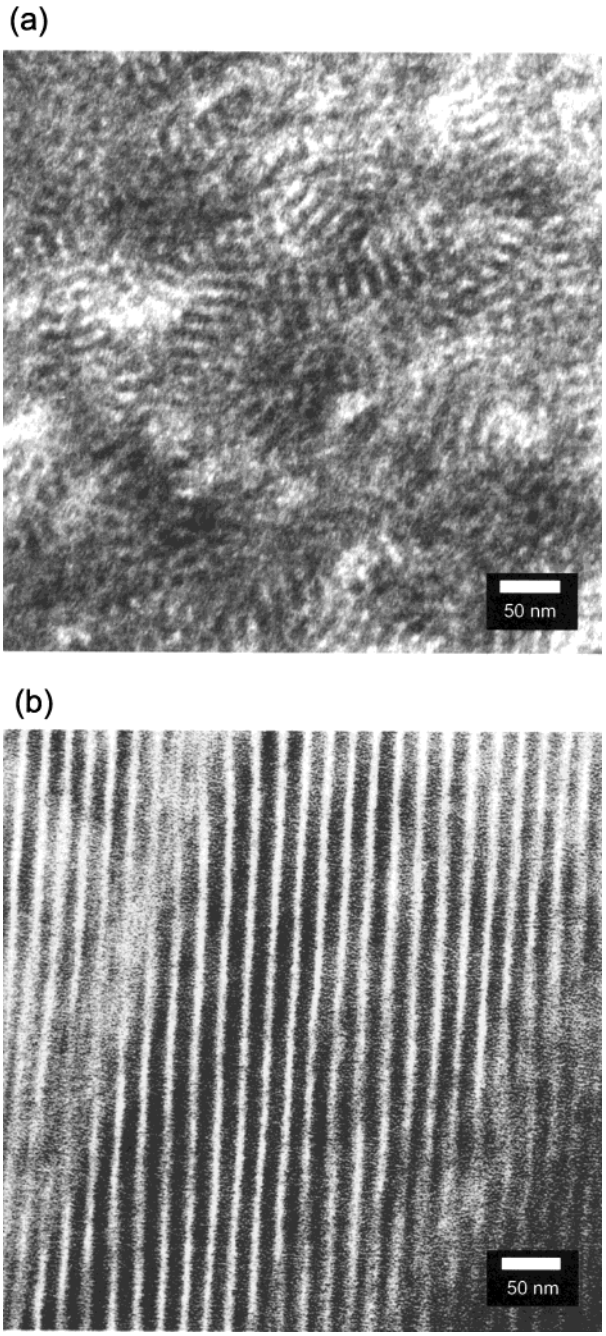


**Figure 7.** TEM micrographs of a compression-molded and a shear-aligned sample of CECEC. Staining with $RuO_4$ leaves the semicrystalline domains of polyethylene dark and the glassy domains of poly(cyclohexylethylene) light. (a) Regularly layered grains of approximately 50 nm in size evidence the short-range translational order in the compression-molded, unaligned sample. (b) Long-range perpendicular order exceeding 1 $\mu$m is evident in the shear-induced specimen. The structure is viewed along the shear direction and shows the regular organization of lamellae in the ($y$,$z$) plane.

in Figure 8a are three SAXS patterns obtained from this sample with the incoming beam directed along the $x$, $y$, and $z$ axes (see top illustration in Figure 1). Circular plots ($I_{q^*}(\phi)$ vs $\phi$) of each pattern are shown in Figure 8, parts b−d. The presence of two intense points of scattering in reciprocal space along the $z$ direction suggests a single-crystal-like alignment of the structure. The first-order reflection at $q^*$ was accompanied by higher order diffraction at $2q^*$ and $3q^*$ (not illustrated). To obtain a real space image of the structure the

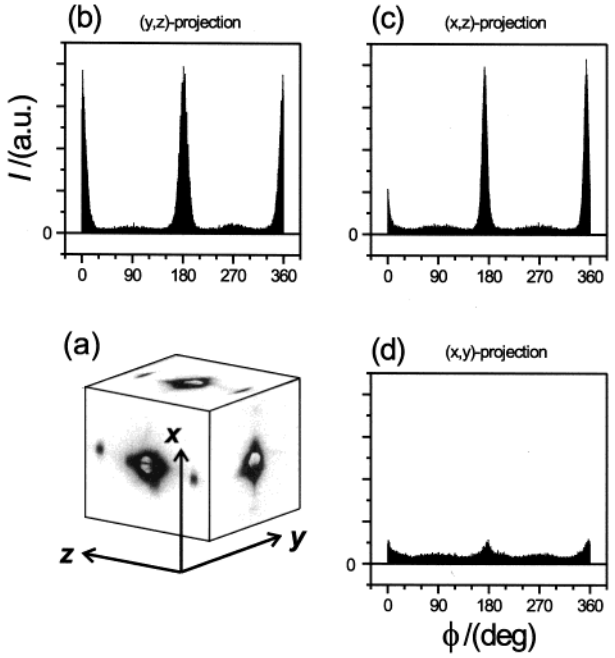


**Figure 8.** SAXS analysis of shear-induced lamellae orientation. Two-dimensional scattering patterns were obtained in the three orthogonal directions ($x$, $y$, and $z$). (a) The two-dimensional data are illustrated in three-dimensional reciprocal space, and related to the shear coordinate system. Nearly all scattering from the sample is concentrated in two Bragg points along the $z$-direction. (b−d) The circular plots of the SAXS patterns of each projection are shown on the same linear intensity scale. The $z$ direction marks the zero angle ($\phi = 0$) in parts b and c, while the $y$ direction marks the zero angle in part d. This SAXS data are consistent with the assignment of a perpendicular lamellar orientation.

specimen was microtomed along the ($y$,$z$) plane, stained, and analyzed by TEM. Figure 7b shows the micrograph which reveals a well-aligned lamellar morphology over length scales of macroscopic order (> 1 $\mu$m). Indeed the results presented in Figures 7b and 8 prove that shearing has created perpendicular lamellae.

**3.2.3. Temperature and Shear Rate Limits of Perpendicular Lamellae.** The perpendicular lamellar orientation was shear-induced by quenching the sample from disorder as described in the previous section. This guaranteed reproducibility and offered the possibility of using the same specimen for a series of different experiments by erasing any sample history through disordering. The range of stability of the perpendicular lamellae was evaluated by scanning either temperature (at 1 °C/min) or shear rate $\dot{\gamma}$ (in steps of 2 $s^{-1}$) and recording changes in the 2D SANS patterns. Four trajectories through ($T$, $\dot{\gamma}$) space were analyzed. The perpendicularly aligned sample was either heated at constant shear rates (0, 1, and 5 $s^{-1}$) or exposed to increasing values of shear rate at 183 °C.

The static heating run ($\dot{\gamma} = 0$ $s^{-1}$) resulted in the loss of equatorial Bragg reflections at $T = 211 \pm 1$ °C, which we associate with $T_{ODT}$. This agrees well with the $T_{ODT}$ that was determined by rheology (see Figure 4). Heating the sample while applying a shear rate of $\dot{\gamma} = 1$ $s^{-1}$ resulted in the same value for $T_{ODT}$. When using a shear rate of $\dot{\gamma} = 5$ $s^{-1}$ the measured ODT dropped slightly to $T = 209 \pm 1$ °C, which shows that the transition temperature is almost independent of shear rate for rates below 5 $s^{-1}$.

To check for stability with respect to shear rate, the sample was subjected to a series of increasing shear

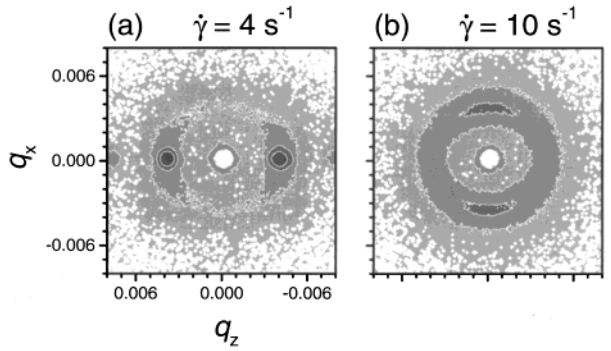


**Figure 9.** Two-dimensional SANS patterns obtained at two shear rates at $T = 183$ °C. (a) $\dot{\gamma} = 4\ s^{-1}$ yielded equatorial Bragg reflections associated with perpendicular lamellae. (b) $\dot{\gamma} = 10\ s^{-1}$ produced a ring of scattering with weak meridional anisotropy interpreted as a shear-disordered state. Intensities are plotted on the same logarithmic scale with one contour level per decade.

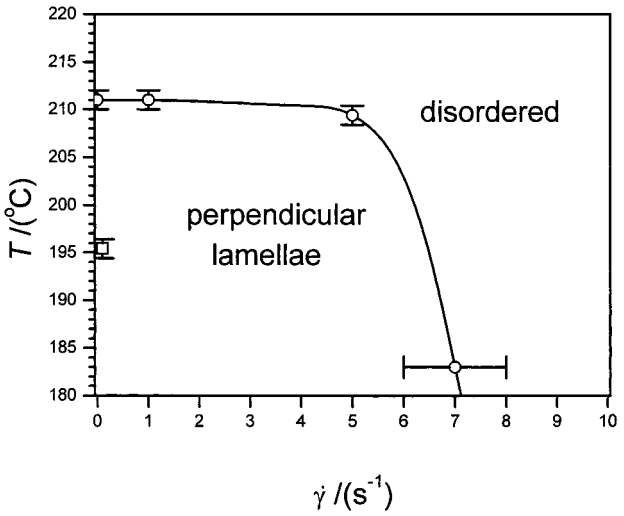


**Figure 10.** Phase portrait ($T_{ODT}(\dot{\gamma})$ vs $\dot{\gamma}$) showing the steady-state structure of CECEC when subjected to $\gamma = \pm 600\%$ reciprocating shear. The full line is a guide to the eye. The transition to the disordered state (circles) was identified by the loss of well-resolved Bragg scattering from the perpendicular lamellae. A transition from the disordered state to perpendicular lamellae (square) was obtained upon cooling (1 °C/min) while shearing ($\dot{\gamma} = 0.1\ s^{-1}$).

rates ($\dot{\gamma} = 2$, 4, 6, 8, and 10 $s^{-1}$) at $T = 183$ °C, well below the static ODT. Figure 9 shows two representative scattering patterns obtained at $\dot{\gamma} = 4$ and 10 $s^{-1}$. These images are qualitatively different in two ways: The intense Bragg reflections convert into a ring of scattering with broad and weak maxima, and the equatorial scattering symmetry associated with the perpendicular orientation transforms into meridional symmetry, at low and high $\dot{\gamma}$, respectively. A shear rate dependent flip of the lamellae to a predominantly parallel orientation with a small transverse component would agree with the scattering pattern shown in Figure 9b. However, this possibility is ruled out by the results of shear quench experiments and TEM investigations to be described below (see section 3.2.5). Therefore, we associate this transformation, which occurred at $\dot{\gamma} = 7 \pm 1\ s^{-1}$, with a shear-induced order−disorder transition, $T_{ODT}(\dot{\gamma})$.

Equatorial reflections associated with the perpendicular orientation were obtained under all conditions where ordered lamellae formed, regardless of shear rate and temperature applied to the sample. These results are summarized in the steady-state phase portrait depicted in Figure 10.

**3.2.4. Sheared Disordered State.** The SANS signature of the shear-induced disordered state was a ring of relatively weak scattering. However, the scattering pattern showed a peculiar anisotropy (see Figure 9b). To establish that this represents a true steady-state response we devised an alternative experimental path (avoiding the ordered state) to the same conditions.

The temperature was set above the ODT at 213 °C, and the effects of the large amplitude shear were analyzed by comparing the scattering ($I_{q^*}(\phi)$) obtained without and with shear (see Figure 11a). An azimuthally flat profile was obtained without shear (filled symbols) which can be associated with a completely isotropic distribution of composition fluctuations.[37,40] At $\dot{\gamma} = 10\ s^{-1}$ (open symbols) the vertical intensity $I(q_x^*)$ (at $\phi = 90°$ and $\phi = 270°$) is 20% above the level of the horizontal intensity $I(q_z^*)$ (at $\phi = 0°$ and $\phi = 180°$), which equals the intensity level measured without shear. A subtle but reproducible shift in the peak wave vector $q_x^*$ is also evident as shown in Figure 11b, where the peak in the vertically scattered intensity from the sheared sample (dotted line) lies approximately 3% lower than the peak of the unsheared data (full line) at $q_x^*(\dot{\gamma} = 0) = 0.0372 \pm 0.0006$ Å$^{-1}$. In contrast, there is no apparent shift in $q_z^*$ without and with shear (circles and crosses, respectively).

Figures 9b and 11a show the same anisotropy of the disordered state of the polymer at a shear rate $\dot{\gamma} = 10\ s^{-1}$, but at two different temperatures: 183 °C (below the static ODT) and 213 °C (above the static ODT). To match up these data and to confirm that the state of the sample is related at these two temperatures, a cooling while shearing experiment was conducted. Beginning at $T = 212$ °C and shear rate $\dot{\gamma} = 10\ s^{-1}$, two-dimensional SANS data were collected while cooling to 183 °C. The cooling produced an increased anisotropy between the vertical intensity $I(q_x^*)$ (squares) and the horizontal intensity $I(q_z^*)$ (circles) as shown in Figure 12a. At the end of this cooling procedure the vertical intensity $I(q_x^*)$ was more than twice the value of the horizontal intensity $I(q_z^*)$. Figure 12b shows the change in the magnitude of the vertical (squares) and horizontal (circles) components of the scattering peak vector ($q_x^*$ and $q_z^*$). The relative shift in peak position increases during cooling. The vertical component $q_x^*$ is about 10% smaller than the horizontal component $q_z^*$ at 183 °C. During cooling $I(q^*)$ and $q^*$ change monotonically, without any evidence of discontinuity, consistent with a continuous disordered thermodynamic state. This experiment also showed consistency between SANS data (see Figures 9b, and 12 at 183 °C) obtained following different processing routes through temperature−shear rate space to the same point ($T = 183$ °C, $\dot{\gamma} = 10\ s^{-1}$) indicating that this reflects the steady state structure.

**3.2.5. Transverse Alignment.** To test how the anisotropy of the disordered state at high shear rate affects the isotropic-to-lamellae transition of the pentablock, we employed a previously described shear jump technique.[22] The scattering from the disordered state while shearing at $T = 183$ °C and $\dot{\gamma} = 10\ s^{-1}$ is reproduced in Figure 13a. Following 3 min at this temperature (with no change in the scattering pattern) the shear was abruptly turned off ($\dot{\gamma} = 0\ s^{-1}$). Figure

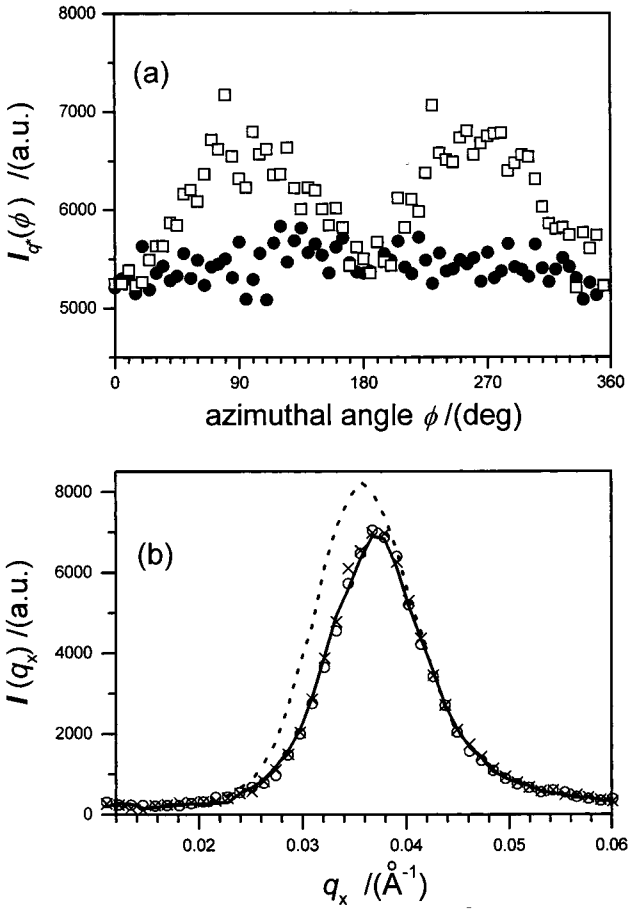


**Figure 11.** Comparison of the SANS intensity from the static ($\dot{\gamma} = 0$ s$^{-1}$) and sheared ($\dot{\gamma} = 10$ s$^{-1}$) states of CECEC at $T =$ 213 °C. (a) Circular plot of the static data (filled circles) shows an isotropic profile of constant intensity. The circular plot of the sheared data (open squares) reveals shear-induced anisotropy of the scattering pattern, with peak intensities along the shear direction $x$ ($\phi = 90°$ and $\phi = 270°$). (b) Radial plots of the scattering without and with shear (along the $x$ direction) show a shift in $q_x^*$ while shearing (dotted line) as compared to the static scattering (full line). Radial plots of the scattering (along the $z$ direction) without (open circles) and with shear (crosses) are also shown, which both coincide with the static $q_x^*$ peak.

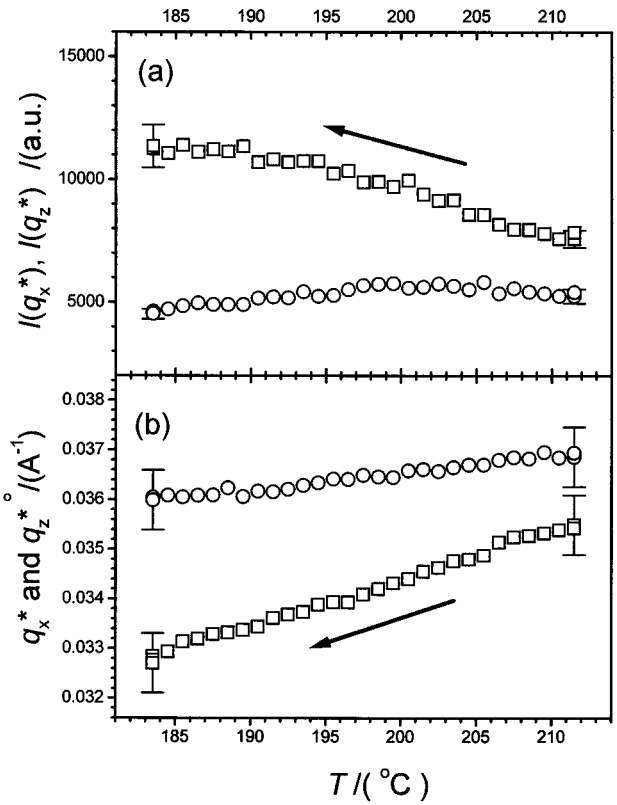


**Figure 12.** Scattering from the disordered sheared state ($\dot{\gamma} = 10$ s$^{-1}$), while cooling from 212 °C to 183 °C at 1 °C/min. The anisotropy of $I(q^*)$ and the relative shift of $q^*$ is illustrated by comparing values along the $x$-axis ($I(q_x^*)$) to values along the $z$-axis ($I(q_z^*)$). (a) The scattering anisotropy is enhanced by cooling as $I(q_x^*)$ (squares) increases to more that twice the value of the unsheared intensity level at 212 °C, while $I(q_z^*)$ (circles) remains constant. (b) The relative shift between $q_x^*$ (squares) and $q_z^*$ (circles) also increases during cooling.

1b shows the SANS pattern recorded during the first 60 s of scattering after shearing was stopped. In fact, we obtained qualitative evidence of such scattering after just 10 s, the detector display time, although the data were binned over 60 s increments in order to accumulate suitable counting statistics. The scattering transforms to a set of strong meridional Bragg reflections at $q_x^*$ and $2q_x^*$. The vertical intensity $I(q_x^*)$ increases more than a decade while the horizontal intensity $I(q_z^*)$ drops similarly as a result of the shear quench. At the point of the shear jump the vertical wave vector $q_x$ relaxes back to its original no-shear level. Within experimental error the horizontal value of $q_z^*$ does not change. The scattering pattern of the ($x$,$z$) plane in Figure 13b indicates that the sample has ordered in the "forbidden" transverse lamellae orientation with the layer normal aligned parallel to the shear direction $x$. The SANS data appear to rule out any partial perpendicular alignment of the sample due to the vanishing horizontal intensity $I(q_z^*)$. We repeated this experiment several times with complete reproducibility.

Following transverse alignment, one sample was cooled and removed from the shear apparatus for analysis by TEM. Micrographs of this sample were obtained from two orthogonal projections. An image of the ($x$,$y$) plane with clear evidence of well-aligned (transverse) lamellae is shown in Figure 14a. The arrow indicates the direction of shear applied prior to the quench. Figure 14b shows the TEM picture obtained from a section microtomed along the ($y$,$z$) plane. This represents a projection along the normal of the layered structure, and consistent with our interpretation, no lamellae are seen. The TEM images confirm the transverse orientation of the lamellae. This alignment resulted from shear quenches from the disordered state at $\dot{\gamma} = 10$ s$^{-1}$ and $T = 183$ °C irrespective of prior sample history. A sample that was sheared ($\dot{\gamma} = 10$ s$^{-1}$) at 213 °C, cooled to 183 °C, and then quenched displayed the same SANS signature that we associate with the transverse structure.

However, the transverse lamellae orientation in Figure 13b is not stable to shear. When shearing was resumed, the sample immediately realigned to give equatorial Bragg reflections, which we associate with the perpendicular lamellae. Figure 13c shows the SANS pattern obtained during the first 60 s of scattering after the transverse structure was exposed to shearing at a rate of $\dot{\gamma} = 1$ s$^{-1}$. The reorientation kinetics take place on a shorter time scale than we can resolve with this neutron scattering technique. (Again we observed ap-

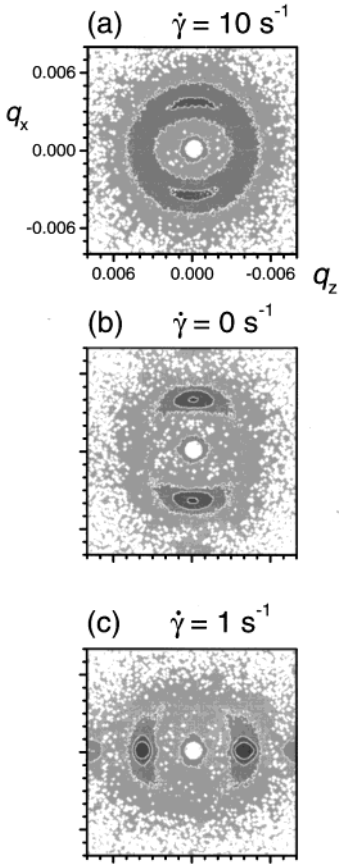


**Figure 13.** Comparison of SANS patterns obtained as a function of processing history at $T = 183$ °C. (a) Steady-state shearing at $\dot{\gamma} = 10\ s^{-1}$ (same data as Figure 9b). (b) Result of shear quenching from (a). Occurrence of meridional Bragg reflections is consistent with transverse lamellae. (c) Data collected during the first 60 s of shear ($\dot{\gamma} = 1\ s^{-1}$) beginning from state b. Equatorial Bragg reflections signal a flip to perpendicular lamellae. SANS intensities are plotted on the same logarithmic scale with one contour level per decade.

parently complete realignment in the first 10 s detector response after the shear device was turned on.) Remarkably, we obtained a similar result with shear rates as low as $\dot{\gamma} = 0.1\ s^{-1}$. At the lower shear rate, realignment was evident after 60 s of shear, which implies essentially complete transformation to the perpendicular form with just 600% of strain (equal to one-quarter of a full shear cycle). This finding confirms that the perpendicular geometry is the steady-state orientation of the CECEC pentablock copolymer.

## 4. Discussion

**4.1 Shear-induced Orientation of the Ordered State.** To understand the shear stability of a lamellar structure in a block copolymer, it is instructive to visualize the effects of a ±600% strain amplitude on the different orientations as shown in Figure 15. Shearing of parallel lamellae is shown in Figure 15a. The lamellar structure is represented by sheets that symbolize the interfaces between layered domains. We have drawn this illustration with the strain distributed homogeneously throughout the structure. However, this arrangement is capable of accommodating mechanical contrast between layers, i.e., one domain is able to flow or deform more easily than the other domain due to differences in entanglement density or proximity to the glass transition.

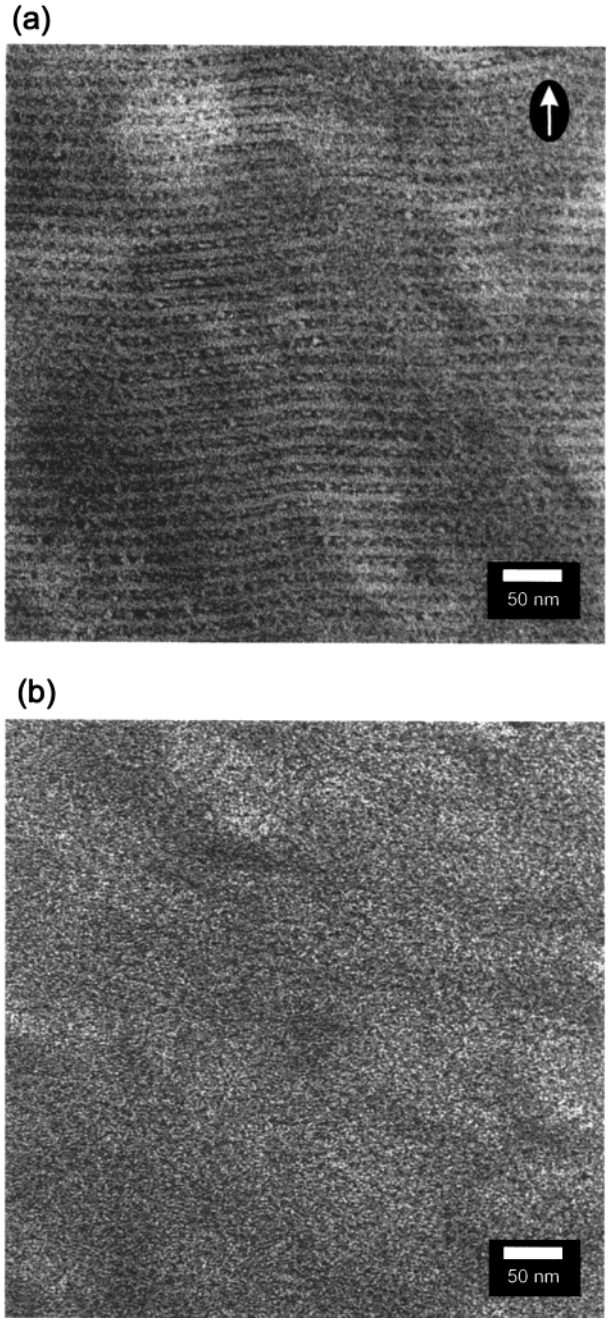


**Figure 14.** TEM micrographs taken from $RuO_4$ stained slices of the CECEC specimen that produced Figure 1b. (a) Sample microtomed in the ($x$,$y$) plane, where the arrow indicates the direction of shear (see Figure 1). (b) Sample microtomed in the ($y$,$z$) plane. Three levels of contrast are evident in these images: Uniform gray (glassy poly(cyclohexylethylene)), nearly white (crystalline polyethylene), and black (amorphous polyethylene). The combination of well-aligned layers (a) and a complete lack of structure (b) is consistent with a transverse lamellae morphology.

Deformation of the transverse—"forbidden"—morphology is illustrated in Figure 15b. Assuming a constant sample density, each lamellar domain must maintain a constant volume during the strain cycle necessitating a reduction in the $d$-spacing as the strain magnitude increases, which will be restricted by the tendency for the polymer blocks to assume random walk conformations. Hence, the transverse structure is not expected to be stable under large amplitude shearing.

Like the parallel orientation, the perpendicular morphology in Figure 15c can maintain a constant $d$-spacing

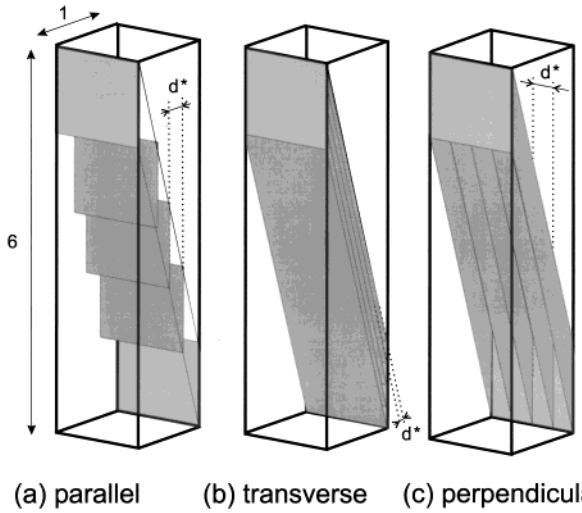


**Figure 15.** Visualization of a ±600% shear strain on the three orthogonal orientations of the lamellar mesophase. (a) In the parallel orientation, the layered domains can slide past each other during shearing without effecting the *d*-spacing. (b) Assuming constant sample density, shearing will change *d* in the transverse structure. (c) Shearing the perpendicular orientation rotates the lamellae without changing the *d* spacing. Only part c can accommodate fully mechanically coupled lamellae.

during shear. However, this arrangement will not necessarily best accommodate lamellae with (extreme) mechanical contrasts, since all domains must sustain the same degree of deformation. In the limit of one stiff and one soft domain, a much higher shear stress will result from the perpendicular than the parallel orientation. This forms the basis for rationalizing the selection of parallel lamellae in certain triblock copolymers.[23,26] However, shearing involves no relative displacement of perpendicular layered domains, and this likely explains why the perpendicular orientation is the shear stable arrangement for pentablock lamellae. In the CECEC pentablock copolymer, the chain architecture dictates that all domains contain blocks that reside in either the bridged conformation or, if looped, then probably entangled. This effectively stitches together all the domains with covalently bonded blocks, yielding a mechanically fully coupled nanocomposite (See Figure 2c). Since none of the domains can slide relative to each other, the parallel orientation is not plausible. The perpendicular morphology permits deformation of the lamellae without significant conformational distortion of bridging and entangled looping chain segments. Thus, the perpendicular orientation can be rationalized as uniquely stable to large amplitude shear in lamellae forming pentablock copolymers.

Shear-induced alignment of diblocks below $T_{ODT}$ is complex and the selection of a steady state parallel or perpendicular orientation is frequency and temperature dependent. However, the kinetics involved are relatively slow with typical times of hours of shearing before long-range alignment develops.[41,42] In this context, it is remarkable how fast the well-aligned state is obtained for the CECEC sample. After only 10 s of shearing the perpendicular orientation is created (see Figure 6b). The SANS experiments do not offer the possibility of time resolution of the alignment process but only document the final effect of shearing the unaligned ordered state. The main difference between this work and shear studies of diblock copolymers by other groups is the value of shear strain, which typically is $|\gamma| < 100\%$. We used $|\gamma| = 600\%$, which could influence the times required to reach steady state. Tepe et al.[23] used $|\gamma| = 600\%$ in their study of shear alignment of PEP−PEE−PEP triblock and reported orientation times of 10 min or longer under similar rheological conditions. This is an order of magnitude faster than the typical time needed for aligning PEP−PEE diblocks,[4] but is still 1 or 2 orders of magnitude slower than the response time of the pentablock in this study. Many mechanisms have been suggested for the shear alignment of lamellar diblock copolymers,[4,10,12,13,17] and the response of lamellae diblocks to shear in the ordered state is a complex combination of elastic deformation and viscous flow.[15,43] At this point, we do not have a clear understanding of the mechanisms responsible for shear alignment of pentablock copolymers, but we conclude that the pentablock responds to shear in a fundamentally different manner than di- and triblock copolymers, based on the drastically reduced response time. Toward the end of this discussion we will present some speculations on this issue, that relate shear behavior to molecular architecture.

**4.2. Shear-Stability of Perpendicular Lamellae−ODT Dependence on Temperature and Shear Rate.** The shear-stable behavior of the CECEC pentablock copolymer with respect to temperature and shear rate is illustrated in Figure 10. Only a single orientation, the perpendicular state, was observed when shearing the ordered state. Furthermore, there was no experimental evidence of shear-induced ordering above $T_{ODT}(\dot{\gamma} = 0)$ in the pentablock, as reported for diblock copolymers.[20] Instead the pentablock exhibits shear-induced disorder as illustrated in Figure 10. Similar shear dependency of the ODT was seen for the triblock studied by Tepe et al.,[23] although in that case it was a parallel-to-disorder transition.

Tri- and pentablock copolymers both display shear-induced disordering, while diblocks show shear-induced ordering. The shear rate at the point of disordering $\dot{\gamma}_{ODT}(T)$ when normalized by the crossover frequency $\omega_x(T)$ (taken at the same temperature $T$), yields roughly $\dot{\gamma}_{ODT}/\omega_x \approx 0.05$ for the PEP−PEE−PEP triblock[23] and $\dot{\gamma}_{ODT}/\omega_x \approx 1$ for the CECEC pentablock. Thus, on a relative time scale, it seems that the shear stable orientation of the pentablock is more robust than that of the triblock. Orientations differ in the two cases, and the apparent greater stability of CECEC may reflect the fact that the rotational component of the shear does not tend to distort perpendicular lamellae, while it will rotate parallel lamellae. Because orientations are different, the shear-disordering mechanisms are also likely to be different. Shear-induced disordering in the PEP−PEE−PEP triblock takes place in the frequency regime well below $\omega_x$, where the individual polymer blocks are dynamically relaxed. In the pentablock, disordering happens at frequencies comparable to the time of single chain relaxation. Therefore, the shear-induced disordering process may reflect a displacement of individual chains by pulling C segments into E domains and vice versa. Another indication that the disordering mechanisms are different in these multiblock systems is qualitatively different neutron scattering from the sheared disordered states, which will be discussed in section 4.4. In both the triblock and pentablock materials a continuous path was established between the static isotropic state ($T > T_{ODT}(\dot{\gamma} = 0)$) and the sheared disordered state well below $T_{ODT}(\dot{\gamma} = 0)$ (see Figure 12),

which verifies the interpretation of shear-induced disordering.

**4.3. Shear-induced Perpendicular Alignment Obtained from the Disordered State.** Formation of the perpendicular state during cooling while shearing is a common feature to all the lamellae-forming block copolymers investigated to date, i.e., the AB, ABA, and ABABA architectures. Koppi et al.[20] found perpendicular lamellae when cooling a nearly symmetric PEP−PEE diblock copolymer from the disordered isotropic state. Tepe et al.[23] found perpendicular lamellae when cooling a PEP−PEE−PEP triblock copolymer from the disordered state, although the parallel orientation was the steady-state morphology once in the ordered state. (Preliminary results with a CEC triblock copolymer are consistent with the data published on PEP−PEE−PEP triblocks; i.e., perpendicular lamellae are obtained when cooling from the disordered state at low shear rates, and parallel lamellae result from shearing the ordered material under all experimental conditions.[44]) Well-aligned states have also been obtained for other block copolymer microphases when cooling from disorder while shearing.[21] This class of ordering phenomenon is explained by the Cates-Milner mechanism[24] of anisotropic suppression of composition fluctuations in the disordered state along the shear direction ($x$) and the direction of the shear gradient ($y$) (see Figure 1). The remaining composition fluctuations, which contribute to scattering along wave vectors parallel to the neutral direction ($z$), become increasingly coherent as the disordered system approaches the limit of stability upon cooling. The result is selection of the perpendicular lamellar alignment resulting in a divergence in $I(q_z^*)$, i.e., Bragg scattering. This theory is not based on a particular chain architecture, but only relies on an overall Brazovskii-type[45] order parameter representation of the segment density. In the low frequency limit ($\dot{\gamma} \ll \omega_c$) the thermodynamics of block copolymers appear to be independent of architecture as di-, tri-, and pentablocks exhibit esentially identical order−disorder hysteresis loops (see Figure 4 and Refs. 37 and 46). Thus, supercooling of the disordered phase displayed by di-, tri-, and pentablock copolymers in this limit suggests a similar shear response in the disordered state, as deduced by Cates and Milner. The disordered melt is dominated by composition fluctuations. Individual chains can still relax, hence they (and their architecture) play no role in how the system responds. As the material is cooled the first element of added stress (associated with composition fluctuations) reflects the collective response of multiple domain periods, not individual chains. Our work establishes this important point of similarity in shear behavior (in the low-frequency limit) for all linear block copolymers in the disordered state, regardless of architecture.

**4.4. Transverse Symmetry of the Anisotropic Disordered and Aligned Ordered States**

Passing through the isotropic-to-order transition via a shear quench yields a dramatically different state than what is obtained upon cooling while shearing at low $\dot{\gamma}$ as discussed in the previous section. The formation of the well-aligned transverse state upon cessation of shearing at 183 °C is a direct consequence of the anisotropy of the composition fluctuations evident in the sheared disordered state prior to shear quenching. The meridional symmetry, with higher intensities along $q_x$, in the SANS pattern in Figures 9b and 13a is qualitatively different from that reported earlier by Hajduk et al.[22] and Tepe et al.[23] for the symmetric PEP−PEE−PEP system. Shear induced disordering of the triblock resulted in composition fluctuations that yielded equatorial scattering symmetry, with higher intensities along the $z$ axis. Subsequent shear quenches at temperatures well below the static ODT led to the spontaneous growth of well-aligned perpendicular lamellae.[22] Thus, the Milner−Cates scenario for the suppression of composition fluctuations in the disordered state in all but the $q_x$ direction in reciprocal space, appears to follow $T_{ODT}(\dot{\gamma})$ to relatively low temperatures ($T - T_{ODT}(\dot{\gamma} = 0) \leq 30$ °C) in triblocks. In contrast, increasing $\dot{\gamma}$ transforms the fluctuation symmetry in the CECEC disordered melt from equatorial ($\dot{\gamma} \leq 1\ s^{-1}$) to meridional ($\dot{\gamma} \simeq 10\ s^{-1}$) as $T_{ODT}(\dot{\gamma})$ is tracked down in temperature (see Figure 10). We believe these differences can be rationalized based on the relative applied shear rate $\dot{\gamma}/\omega_x$. Since $\omega_x$ is inversely proportional to the single chain relaxation time $\tau$, the ratio $\dot{\gamma}/\omega_x$ is simply proportional to the Deborah number, $De = \dot{\gamma}\tau$. Previous experiments with PEP−PEE−PEP have been restricted to $\dot{\gamma}/\omega_x \ll 1$, where single chain dynamics are not accessed, consistent with the Cates−Milner mechanism in the disordered state. Although we do not understand in detail why perpendicular pentablock lamellae are stable at considerably higher reduced shear rates than parallel triblocks, the shear-induced disordered pentablock molecules must be stretched since $\dot{\gamma}_{ODT}/\omega_x \approx 1$. Apparently the combined effects of chain stretching and composition fluctuations are manifested in the meridional anisotropic SANS pattern shown in Figure 13a. We are not aware of any theory that anticipates this result. However, we speculate that large amplitude shearing experiments with ABA−and even AB−block copolymers in the limit $\dot{\gamma}/\omega_x \approx 1$ would result in a similar behavior since the disordered state response to shear should be universal (i.e., independent of architecture), when single chain dynamics dominate the viscoelastic response.

Sketches of the postulated CECEC pentablock molecular conformations under four conditions of temperature and shear rate are shown below the corresponding SANS data in Figure 16. Our cartoons of the pentablock copolymer are course-grained, with blobs representing each block of the molecule. In the static disordered state (panel **a**) all molecules possess random conformations with no preferred orientation. The ring of scattering reflects isotropic composition fluctuations at $q^*$. Applying a high shear rate ($\dot{\gamma} \approx 10\ s^{-1}$) and cooling the sample to 183 °C has two consequences (see Figures 11 and 12): The intensity is enhanced at $q_x^*$ and the magnitude of $q_x^*$ is reduced by about 10% relative to $q_z^*$. In the shear direction the slightly smaller value of $q_x^*$ suggests chain stretching (panel **b**), which could explain the experimental SANS result. The higher meridional intensity and shift to lower $q_x^*$ are consistent with molecular alignment along the shear direction $x$.

When the sample is shear quenched from situation **b** in Figure 16, it instantly orders either by homogeneous nucleation and growth or spinodal decomposition. (We have not been able to establish with certainty whether shear quenches deep into the ordered region results in spinodal decomposition or not.[22]) The anisotropy created in the disordered state controls the orientation of the ordered material (panel **c**). Apparently the ordering kinetics deep in the ordered state are faster than the time required for chain relaxation ($\tau$). Thus, the trans-

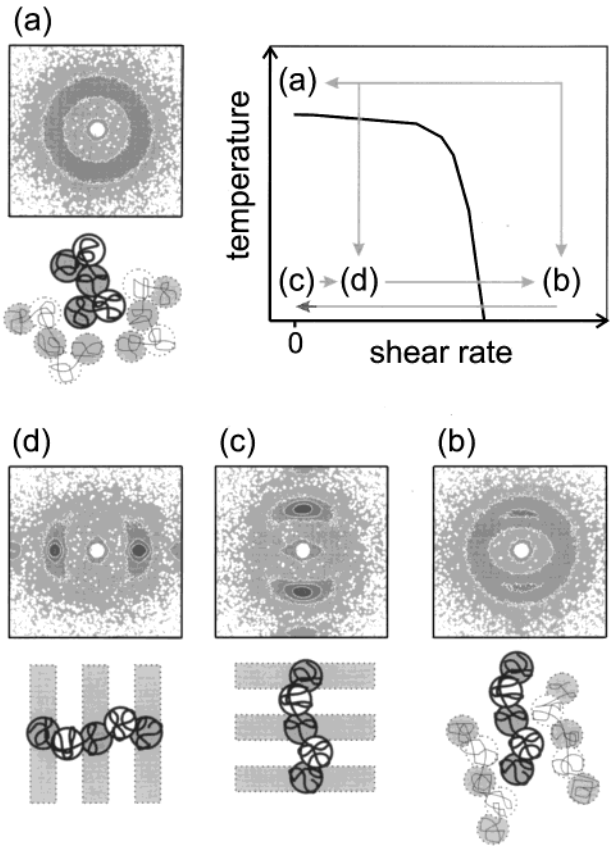


**Figure 16.** Speculated effects of shear on the molecular conformation of the CECEC pentablock copolymer. Four experimental conditions are marked as points a−d in the schematic ($T$ vs $\dot{\gamma}$) diagram. The SANS pattern at each condition is shown in the panel below together with coarse-grained cartoons of plausible molecular conformations.

verse lamellar morphology reflects the state of CECEC chain stretching present at 183 °C and 10 $s^{-1}$.

A fundamentally different set of concepts explain the fourth state illustrated in Figure 16 (panel **d**). We have already described how mechanical contrast and the Cates−Milner mechanism drive selection of perpendicular lamellae in the ordered state and disordered states, respectively. Because there is some tendency for bridged block conformations, the net molecular alignment will be partially coincident with the lamellar normal as illustrated in Figure 16d. Although we have not yet determined the extent of chain orientation, we suspect perpendicular alignment forces a much stronger conformational bias than would be anticipated under static equilibrium condition. We speculate that such a "log rolling" type of alignment with a predominance of chains in bridged conformations directed along the $z$ direction would be less susceptible to the effect of shear. Looping chain conformations, which directs the chain contour mostly along the $x$ and $y$ directions, would complicate the accommodation of large shear strain. (Metaphorically, entangled hairpins will offer more resistance to flow than straightened rolling hairpins). If correct, such chain orientation could have significant effects on the solid-state mechanical properties.

**4.5. Mechanisms of Shear-Alignment below ODT.** As noted in section 4.1 the CECEC pentablock displays a remarkable rapid response time for shear-alignment ($t \leq 10$ s). The pentablock architecture results in the mechanical coupling of all domains throughout the sample (see Figure 2c), which effectively excludes dissipation of shear stress through sliding of grain boundaries or viscous flow within the central region of the microdomains. The dynamics of domains and grain boundaries alike are influenced by the "molecular stitching" of the lamellae. We believe an imposed shear strain transmits stress throughout the mechanically coupled material, in contrast to what occurs in diblocks and triblocks, where sliding at grain boundaries and within domains is possible. Therefore, we postulate that the mechanism responsible for perpendicular alignment involves disordering of all misaligned portions of the sample followed by spontaneous growth, analogous to what occurs during the cooling while shearing from the disordered state. Since $\tau \approx \omega_x^{-1} \approx 0.1$ s (see Figure 5 with temperature correction), disordering followed by reordering would be feasible within the 10 s transformation time identified by SANS (see Figures 6 and 13). Taken together, these findings and our interpretations suggest a unique alignment mechanism for the ordered but unaligned symmetric pentablock copolymer, with an unprecedented rapid response to large amplitude shear. This fact, that processing affects the lamellar morphology on a time scale of seconds (and not hours, as for diblocks), may be an important property of pentablock copolymers for future applications.

**4.6. Comparison with Other Studies.** Within the broader context of soft materials there are many examples of shear-induced alignment of morphology including studies of thermotropic and lyotropic liquid crystals, as well as block copolymers. Here we comment on a few relevant cases.

Alignment of chains in the flow direction is commonly observed in thermotropic liquid crystalline polymers (LCP) at high shear rates and/or temperatures. Romo-Uribe and Windle[47,48] have reported a flip in alignment from "log-rolling" (director perpendicular to the shear and gradient directions) at lower shear rates to "flow-alignment" (molecules aligned parallel to the flow) at higher shear rates. The authors associate this transition with a segregation of short similar blocks in the random (block)copolymer liquid crystal that is compatible with shear at low rates. In another multiblock LCP, Zhou et al.[49] measured a similar transition of the molecular alignment between a possible smectic phase of log-rolling molecules, and a nematic state of flow-aligned molecules. These examples of transitional behavior bear resemblance to what we report here for the $T_{ODT}(\dot{\gamma})$ of CECEC. There is direct evidence of flow alignment in both systems at high shear. However at low shear rates, the layered or smectic nature is somewhat speculative for LCP, while it is well documented for the pentablock copolymer by SANS, SAXS, and TEM. On the other hand these LCP studies provide direct evidence of single chain alignment via wide-angle X-ray scattering, which derives from inter-stem correlations. In the pentablock work reported here we do not have similar direct data, but can only infer the state of chain orientation based on correlation hole scattering at $q^*$.

Leist et al.[50] have reported on alignments of a lamellar PS−PI block copolymer induced by extrusion through a rectangular slit die, followed by a quench to room temperature. Although the polymer was subjected to an ambiguous combination of extensional and shear flows, this processing establishes experimental conditions that must reach into the $\dot{\gamma}/\omega_x \approx 1$ limit. Indeed, extrusion at high shear rates resulted in a morphology that gave SAXS data implying a destruction of the

lamallar structure—analogous to the shear-induced disordering displayed by the PEP−PEE−PEP triblock and CECEC pentablock copolymers. Subsequent annealing (at $T > T_g$(PS)) led to the formation of perpendicular lamellae, which the authors speculate is due to a chain orientation along the vorticity direction of the slit die flow. However, our findings (of flow-aligned chains in the disordered state) contradicts this hypothesis.

The transverse structures reported in diblock copolymers typically coexist with parallel lamellae.[13,17,18,19] Zhang et al.[15,17] claimed a "pure" transverse alignment at low amplitude oscillatory shear ($|\gamma| = 8\%$ and $T \ll T_{ODT}$), and suggested that chain orientation plays a role in the formation of transverse vs parallel lamellae. Although our experiments are fundamentally different ($|\gamma| = 600\%$ and $T \approx T_{ODT}$), we have drawn a similar conclusion regarding the role of chain alignment in controlling lamellae orientation at high rates of deformation.

## 5. Summary

We have investigated the shear-induced structures of a compositionally symmetric CECEC pentablock copolymer near the order−disorder transition. Application of a large amplitude ($|\gamma| = 600\%$) steady reciprocating shear deformation led to the rapid development of well-aligned perpendicular lamellar when $\dot{\gamma}\tau < 1$ where $\tau$ is the single chain relaxation time. When $\dot{\gamma}\tau > 1$ the material disorders, displaying an azimuthally asymmetric SANS pattern with weak broad maxima situated along the shear direction. This unusual result is interpreted as evidence of macromolecular alignment in the shear-disordered state. Cessation of shearing 30 °C below $T_{ODT}(\dot{\gamma} = 0)$ resulted in the spontaneous transformation of the anisotropic disordered melt into well-aligned lamellae with a transverse (i.e., "forbidden") orientation, consistent with this chain stretching hypothesis.

These findings were considered in the context of previous studies that dealt with AB diblock and ABA triblock copolymers, with particular emphasis on the concept of mechanical coupling. The pentablock architecture imposes a uniformly strong mechanical coupling between different lamellar microdomains through bridging and entangled looping block conformations, thereby eliminating mechanical contrast for $\dot{\gamma}\tau < 1$. As a consequence, the perpendicular orientation is the only stable arrangement under large strains. In sharp distinction, a large mechanical contrast in ABA triblocks results in the parallel alignment, while a variable mechanical contrast in diblocks can produce either perpendicular or parallel lamellae. We speculate that these differences in steady-state alignment also influence the condition for shear disordering where $(\dot{\gamma}\tau)_{ODT} \approx 1$ and 0.1 for (perpendicular) pentablocks and (parallel) triblocks, respectively. In the opposite limit, $\dot{\gamma}\tau \ll 1$, all three linear architectures develop perpendicular lamellae when specimens are cooled below $T_{ODT}$, which we interpret as direct support for the Cates−Milner mechanism of anisotropic suppression of composition fluctuations.

**Acknowledgment.** This work was supported by the Dow Chemical Co. and the Division of Materials Sciences, U.S. Department of Energy, under Contract No. DE-AC05-96OR22464 with Lockheed Martin Energy Research Corp. The authors thank Paul Butler and Sungmin Choi for help with SANS experiments at NIST and Elena Dormidontova for helpful discussions. M.E.V. gratefully acknowledges the support of the Carlsberg Foundation (Denmark) and the Danish Technical Research Council.

## References and Notes

(1) Keller, A.; Pedemonte, E.; Willmouth, F. M. *Nature* **1979**, *225*, 538.
(2) Hadziioannou, G.; Mathis, A.; Skoulios, A. *Colloid Polym. Sci.* **1979**, *257*, 136−139.
(3) Hadziioannou, G.; Picot, C.; Skoulios, A.; Ionescu, M.-L.; Mathis, S.; Duplessix, R.; Gallot, Y.; Lingelser, J.-P. *Macromolecules* **1982**, *15*, 263.
(4) Koppi, K. A.; Tirrell, M.; Bates, F. S.; Almdal, K.; Colby, R. H. *J. Phys. Fr. II* **1992**, *2*, 1941−1959.
(5) Winey, K. I.; Patel, S. S.; Larson, R. G.; Watanabe, H. *Macromolecules* **1993**, *26*, 2542.
(6) Winey, K. I.; Patel, S. S.; Larson, R. G.; Watanabe, H. *Macromolecules* **1993**, *26*, 4373.
(7) Kannan, R. M.; Kornfield, J. A. *Macromolecules* **1994**, *27*, 1177.
(8) Zhang, Y.; Wiesner, U.; Spiess, H. W. *Macromolecules* **1995**, *28*, 778.
(9) Fredrickson, G. H.; Bates, F. S. *Annu. Rev. Mater. Sci.* **1996**, *26*, 501−550.
(10) Wiesner, U. *Macromol. Chem. Phys.* **1997**, *198*, 3319−3352.
(11) Chen, Z.-R.; Kornfield, J. A. *Polymer* **1998**, *39*, 4679−4699.
(12) Patel, S. S.; Winey, K. I.; Watanabe, H. *Macromolecules* **1995**, *28*, 4313.
(13) Chen, Z.-R.; Issaian, A. M.; Kornfield, J. A.; Smith, S. D.; Grothaus, J. T.; Satkowski, M. M. *Macromolecules* **1997**, *30*, 7096−7114.
(14) Gupta, V. K.; Krishnamoorti, R.; Chen, Z.-R.; Kornfield, J. A.; Smith, S. D.; Satkowski, M. M.; Grothaus, J. T. *Macromolecules* **1996**, *29*, 875−884.
(15) Zhang, Y.; Wiesner, U. *Macromol. Chem. Phys.* **1998**, *199*, 1771−1784.
(16) Bird, R. B.; Armstrong, R. C.; Hassager, O. *Dynamics of Polymeric Liquids*, 2nd ed.; John Wiley & Sons: New York, 1987; Vol. 1.
(17) Zhang, Y.; Wiesner, U. *J. Chem. Phys.* **1995**, *103*, 4784.
(18) Okamoto, S.; Saijo, K.; Hashimoto, T. *Macromolecules* **1994**, *27*, 5547−5555.
(19) Pinheiro, B. S.; Hajduk, D. A.; Gruner, S. M.; Winey, K. I. *Macromolecules* **1996**, *29*, 1482−1489.
(20) Koppi, K. A.; Tirrell, M.; Bates, F. S.*Phys. Rev. Lett.* **1993**, *70*, 1449−1452.
(21) Almdal, K.; Mortensen, K.; Koppi, K. A.; Tirell, M.; Bates, F. S. *J. Phys. Fr. II* **1996**, *6*, 617−637.
(22) Hajduk, D. A.; Tepe, T.; Takenouchi, H.. Tirrell, M.; Bates, F. S. *J. Chem. Phys.* **1998**, *108*, 326−333.
(23) Tepe, T.; Hajduk, D. A.; Hillmyer, M. A.; Weimann, P. A.; Tirell, M.; Bates, F. S. *J. Rheol.* **1997**, *41*, 1147−1171.
(24) Cates, M. E.; Milner, S. T *Phys. Rev. Lett.* **1989**, *62*, 1856−1859.
(25) Riise, B. L.; Fredrickson, G. H.; Larson, R. G.; Pearson, D. S. *Macromolecules* **1995**, *28*, 7653.
(26) Fredrickson, G. H. *J. Rheol.* **1994**, *87*, 1045−1067.
(27) Gehlsen, M. D.; Bates, F. S. *Macromolecules* **1994**, *27*, 3611−3618.
(28) Fetters, L. J.; Lohse, D. J.; Richter, D.; Witten, T. A.; Zirkel, A. *Macromolecules* **1994**, *27*, 4639.
(29) Young, R. N.; Quirk, R. P.; Fetters, L. J. *Adv. Polym. Sci.* **1984**, *1*, 56.
(30) Gehlsen, M. D.; Bates, F. S. *Macromolecules* **1993**, *26*, 4122−4127.
(31) McManus, N. T.; Rempel, G. L. *J. Macromol. Sci.—Rev. Macromol. Chem. Phys.* **1995**, *C35*, 239.
(32) U.S. Patent 5,612,422.
(33) Koppi, K. A.; Tirrell, M.; Bates, F. S.; Almdal, K.; Mortensen, K. *J. Rheol.* **1994**, *38*, 999−1027.
(34) Tepe, T.; Schulz, M. F.; Zhao, J.; Tirrell, M.; Bates, F. S. *Macromolecules* **1995**, *28*, 3008.
(35) Brown, G. M.; Butler, J. H. *Polymer* **1997**, *38*, 3937−3945.
(36) Chaffin, K. A.; Bates, F. S.; Brant, P.; Brown, G. M. *J. Polym. Sci. B* **2000**, *38*, 108−121.
(37) Almdal, K.; Bates, F. S.; Mortensen, K. *J. Chem. Phys.* **1992**, *96*, 9122.

(38) Rosedale, J. H.; Bates, F. S. *Macromolecules* **1990**, *23*, 2329−2338.
(39) Han, C. D.; Kim, J.; Kim, J. K. *Macromolecules* **1989**, *22*, 383−394.
(40) Fredrickson, G. H.; Helfand, E. *J. Chem. Phys.* **1987**, *87*, 697.
(41) Gupta, V. K.; Krishnamoorti, R.; Kornfield, J. A.; Smith, S. D. *Macromolecules* **1995**, *28*, 4464−4474.
(42) Chen, Z.-R.; Kornfield, J. A.; Smith, S. D.; Grothaus, J. T.; Satkowski, M. M. *Science* **1997**, *277*, 1248−1253.
(43) Polis, D. L.; Winey, K. I.; Ryan, A. J.; Smith, S. D. *Phys. Rev. Lett.* **1999**, *83*, 2861−2864.
(44) Tepe, T. Ph.D. Thesis, University of Minnesota, 1997.
(45) Brazovskii, S. A. *Sov. Phys. JETP* **1975**, *41*, 85.
(46) Tepe, T. Unpublished data.
(47) Romo-Uribe, A.; Windle, A. H. *Macromolecules* **1993**, *26*, 7100−7102.
(48) Romo-Uribe, A.; Windle, A. H. *Macromolecules* **1996**, *29*, 6246−6255.
(49) Zhou, W.-J.; Kornfield, J. A.; Ugaz, V. M.; Burghardt, W. R.; Link, D. R.; Clark, N. A. *Macromolecules* **1999**, *32*, 5581−5593.
(50) Leist, H.; Geiger, K.; Wiesner, U. *Macromolecules* **1999**, *32*, 1315−1317.

MA000709Q